Available online at www.sciencedirect.com
ScienceDirect
Journal of Sound and Vibration 312 (2008) 182–194
JOURNAL OF SOUND AND VIBRATION
www.elsevier.com/locate/jsvi

Theoretical investigation on wireless vibration control of thin beams using photostrictive actuators

Dongchang Sun, Liyong Tong*

School of Aerospace, Mechanical and Mechatronic Engineering, The University of Sydney, Sydney, NSW 2006, Australia

Received 31 August 2007; received in revised form 31 August 2007; accepted 20 October 2007
Available online 11 December 2007

Abstract

This paper presents an investigation into wireless remote vibration control of flexible beams using photostrictive materials and laser Doppler vibrometers. To increase the response speed of photostrictive actuator to light irradiation, a thin lead lanthanum zirconate titanate (PLZT) film with transparent electrodes is bonded onto the host beam as the actuator. A mathematical model is presented to describe the interaction between the motion of the host beam and light-induced strain of the photostrictive actuator. To perform remote wireless control, a laser Doppler vibrometer is used as the sensor to measure the vibrating velocity and the sensing equation that relates output of the vibrometer and velocity of the vibrating beam is presented. A modal velocity filter (MVF) is presented to observe the desired modal velocities, which is fed back to form light intensity of the photostrictive actuator to perform the closed-loop wireless vibration control. A characteristic equation is presented from which the frequencies and active damping ratios for all modes can be evaluated. Finally, a simulation example is given to show the effectiveness of the present model and control scheme.

1. Introduction

Smart structures with distributed actuators made of smart materials such as piezoelectric, shape-memory alloy, and electrostrictive liquids have been extensively studied [1,2]. Since the distributed sensors, actuators, and control systems are either embedded or surface-bonded in these structures, hard-wire connections are required to transmit sensing signals and control commands. Hard-wire connections often attract electric noise, which will contaminate the sensor and control signals and degenerate the distributed control. In addition, hard-wire connections may not be feasible or desirable in hostile environments and applications. For instance, the presence of external wires connected to a robot will seriously affect its mobility. Accordingly, optically driven and remotely actuated actuators are advantageous in these situations.

The photo-driven materials, which are capable of converting photonic energy to mechanical motion, have potential applications in wireless remote actuation, remote sensing and remote control of smart structures and machines. Among the photo-driven materials, photostrictive materials have attracted a wide research in materials engineering and have great potential in applications of remote structural vibration control.

*Corresponding author. Tel.: +61 2 93516949; fax: +61 2 93514841.
E-mail address: ltong@aero.usyd.edu.au (L. Tong).

0022-460X/$ - see front matter © 2007 Elsevier Ltd. All rights reserved.
doi:10.1016/j.jsv.2007.10.049

The mechanism of photostrictive effect is a combination of the photovoltaic and the converse piezoelectric effects. When the photostrictive materials, such as lead lanthanum zirconate titanate (PLZT) ceramic, are illuminated by light with certain wavelength, a high voltage up to the order of kV/mm is generated. This high photovoltage then induces mechanical strain due to the converse piezoelectric effect of the photostrictive materials.

Research on photo-driven materials focuses initially on the enhancement of the photostrictive effect of materials by controlling and optimizing processing methods, ceramic composition and dopant type/content in recent years [3,4]. The strain of this kind of materials induced by light reaches 0.05–0.1%, which is about a half of strain level induced by electric field in widely used piezoelectric materials. As the improvement in the photostrictive effect of the photostrictive materials, their applications have been also explored based on experimental investigations. Fukuda et al. [5] tested the actuating behavior of a bimorph PLZT element irradiated on both sides of the bimorph to increase the response speed to the light irradiation. They also designed and tested an optical servo system using bimorph PLZT. Uchino [6] developed a photo-driven relay and a micro-walking device using a bimorph configuration, which had neither electric lead wires nor electric circuits. Morikawa and Nakada [7] proposed an effective position control method for the bimorph-type optical actuator and validated it by experiments. Belforte et al. [8] designed and constructed a mechanical micro-actuator activated by a PLZT, which can be amplified by the movement induced in the PLZT via an ultraviolet lamp. Baglio et al. [9] introduced an innovative actuation strategy based on a photo-thermo-mechanical energy transformation and designed an actuator prototype. Kawaguchi et al. [10] tested the photovoltaic voltage and current in a PZLT specimen and an optical motor made of PLZT was designed and tested. A typical experimental setup for the photostrictive materials under light irradiation is shown in Fig. 1 [10].

The existing experimental investigations have shown that the photostrictive materials have the great potential to be used as actuators in wireless structural control [11]. However, the slow response of photostrictive materials to light irradiation, which has to be modelled by a time-dependent constitutive law of photostrictive materials, has limited further applications of photostrictive materials in active vibration control of structures. Fortunately, recent studies show that the response speed of bimorph bulks and films with transparent indium tin oxide electrodes can reach 0.01 s (>100 Hz) [12], which is suitable for lower modal control of flexible structures with lower frequencies. This paper aims to explore the applications of photostrictive materials in vibration control of flexible structures.

This paper presents an investigation into the wireless remote vibration control of beam using photostrictive films and laser Doppler vibrometers. Photostrictive actuating equations is developed for thin beams bonded with photostrictive actuator patches based on an exponential constitutive law of photostrictive materials. Since the light intensity is always positive, two photostrictive actuator films are bonded on the surfaces of the beam so that the control light intensity is positive in the process of the active vibration control. A computational method is presented to determine the eigenvalues of the closed-loop controlled composite beam, and hence the control effectiveness and control stability can be examined.

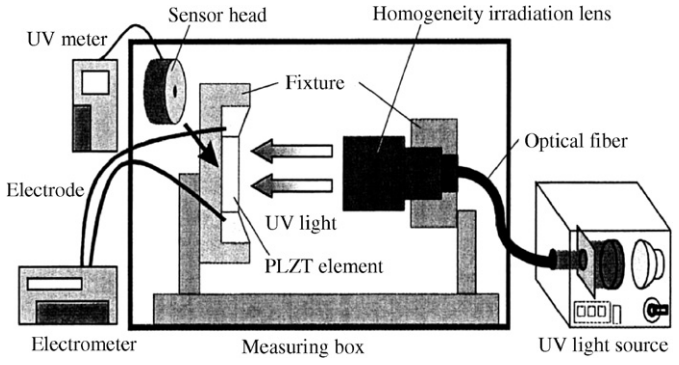

Fig. 1. A typical experiment setup of light irradiation on photostrictive materials [10].

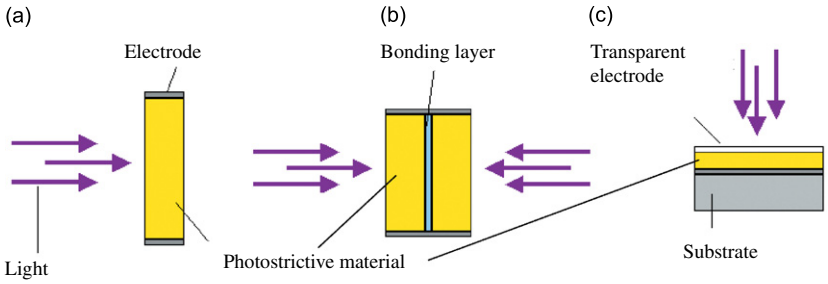

Fig. 2. Three types of photostrictive actuators. (a) Single plate bulk, (b) bimorph bulk, (c) film.

2. Photostrictive actuators

A photostrictive actuator can be a bulk, a bimorph or a film one, as shown in Fig. 2. A bulk photostrictive actuator is made of a photostrictive plate, and its two (small) side surfaces are metallized as two electrodes, while its largest surfaces are used to receive light illumination. The response of the bulk photostrictive actuator to the light irradiation is usually slow, which is suitable to perform static or quasi-static shape control of flexible structures. A bimorph actuator is made of two bulk photostrictive actuators bonded back-to-back using opaque glue. Since the two photostrictive plates can receive two different light inputs, the bimorph actuator has a much quicker response to the light irradiation up to 100 Hz. Since two surfaces of the bimorph actuator need to be exposed to light inputs, it has some limitations to be mounted onto the host structures. A photostrictive film actuator is a thin plate metallized with its largest surface as electrodes. These electrodes are made of transparent electrically conductive material such as indium tin oxide. Therefore, these two metallized surfaces are also used to receive light inputs. Due to the thin layer between the electrodes, the photostrictive actuator film has a quick response of over 100 Hz and suitable for vibration control of several lower and dominant vibration modes of flexible structures.

Since photostrictive effect is the combination of the photovoltaic and inverse piezoelectric effects, the strain induced by light intensity is the product of the photovoltage E_{op} and its piezoelectric coefficient d_{31} or d_{33}. Therefore, the relationship between the photovoltage and the light intensity needs to be established first. Due to the fast response speed of the photostrictive film with transparent electrodes to the light irradiation, we employ a nonlinear exponential model [13] instead of the time-dependent model [11]. In this section, the constitutive relationship between the photo-induced average electric field and the driven light intensity is briefly described as follows [13].

When considering the second-order nonlinear effect, the polarization of dielectrics can be expressed as

$$P = \varepsilon_0(\chi_1 E_{op} + \chi_2 E_{op}^2), \tag{1}$$

where ε_0 is permittivity efficient of vacuum, χ_1 is the linear susceptibility, χ_2 is the nonlinear susceptibility of the second order, and E_{op} is the electric field at a single optical frequency. Replacing E_{op} with the alternating electric field $E_{op}\cos\omega_{op}t$ in Eq. (1), we have

$$P = \varepsilon_0(\chi_1 E_{op}\cos\omega_{op}t + \chi_2 E_{op}^2\cos^2\omega_{op}t), \tag{2}$$

where ω_{op} is the optical frequency. After adding the additional field generated by the polarization charges in the polarized dielectrics, and employing the Lorentz relation [14], the local field in dielectrics can be approximately expressed by

$$E_{local} = E + \frac{\gamma P}{3\varepsilon_0}, \tag{3}$$

where E is the macroscopic electric field and γ is the Lorentz factor. When an alterative electric field with amplitude E_{op} and optical frequency ω_{op} is applied, the local field becomes

$$E_{local} = E\cos\omega_{op}t + \frac{\gamma}{3}(\chi_1 E_{op}\cos\omega_{op}t + \chi_2 E_{op}^2\cos^2\omega_{op}t). \tag{4}$$

The average of the local electric field in Eq. (4) will be:

$$\bar{E}_{\text{local}} = \tfrac{1}{6}\gamma\chi_2 E_{\text{op}}^2. \tag{5}$$

It should be noted that Eq. (5) is derived under a coherent propagation of the light wave at a single frequency. In general cases, this condition of coherent illumination is not satisfied and hence Eq. (5) is modified as

$$\bar{E}_{\text{local}} = c_1\gamma\chi_2(E_{\text{op}}^2)^{\beta}, \tag{6}$$

where c_1 is a constant and $0<\beta\leqslant 1$ is a parameter of the depression effect which can be determined by experiment. Replacing the variable E_{op}^2 with the light intensity I_{op} [13], the average induced (DC) field induced by incoherent light source can be expressed as

$$\bar{E} = \bar{E}_{\text{local}} = c_2\gamma\chi_2 I_{\text{op}}^{\beta}, \tag{7}$$

where c_2 is a constant.

Due to the inverse piezoelectric effect, the strain of the photostrictive material can be expressed as

$$\varepsilon = s\sigma + d_{31}c_2\gamma\chi_2 I_{\text{op}}^{\beta}, \tag{8}$$

where ε is the strain, σ is the stress, s is the elastic compliance, and d_{31} is the piezoelectric strain constant of the material. The second part on the right-hand side of Eq. (8) is the strain induced by the light irradiation. The stress–strain relation of the photostrictive material can also be written in the following form:

$$\sigma = Y\varepsilon - p_{31}I_{\text{op}}^{\beta}, \tag{9}$$

where $p_{31} = e_{31}c_2\gamma\chi_2$ is the photostrictive stress constant, e_{31} is the piezoelectric stress constant, and Y is the Young's modulus.

Eq. (9) describes the contribution of light intensity to overall stress of the photostrictive materials, and it will be used in vibration control of beams in the following sections.

3. Modeling of beams with photostrictive actuators

3.1. Photostrictive actuation equations

Consider a thin beam bonded with a pair of photostrictive film actuators show in Fig. 3. One of these two identical photostrictive actuators is bonded on the upper surface, and the other is bonded on the collocated lower surface. Since the actuation performance of the photostrictive actuators under reasonable light intensity is not strong enough so far, they are usually used to control thin flexible structures or microstructures. Therefore, in the model, the adhesive layer between the film actuator and thin host structure should be considered. As the adhesive layer is much thinner compared to the films and the substrates, the peel and shear

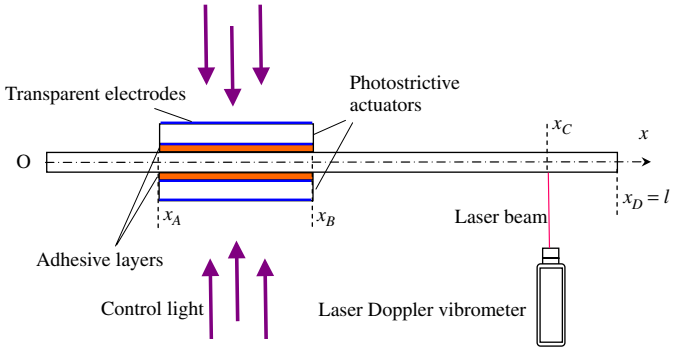

Fig. 3. Beams with photostrictive actuators.

stresses can be assumed to be constant across its thickness. It is assumed that a ventilation system is used so that the temperature of the composite beam remains constant during light illumination. Moreover, the control light is assumed to be uniformly distributed on the surfaces of both photostrictive actuators at any time.

The governing equations of the beam with and without photostrictive actuators are different and will be presented separately. For the beam segment bonded with the photostrictive actuators ($x_A \leqslant x \leqslant x_B$), its free-body diagram is depicted in Fig. 4, and its equations of motion can be obtained as follows:

$$\begin{aligned}
&\rho_1 bh_1 u_{1,tt} = T_{1,x} + b\tau_1, \quad \rho_1 bh_1 w_{1,tt} = Q_{1,x} + b\sigma_1, \quad M_{1,x} + b\tau_1 h_1/2 - Q_1 = 0,\\
&\rho_2 bh_2 u_{2,tt} = T_{2,x} + b(\tau_2 - \tau_1), \quad \rho_2 bh_2 w_{2,tt} = Q_{2,x} + b(\sigma_2 - \sigma_1),\\
&M_{2,x} + b(\tau_1 + \tau_2)h_2/2 - Q_2 = 0, \quad \rho_3 bh_3 u_{3,tt} = T_{3,x} - b\tau_2,\\
&\rho_3 bh_3 w_{3,tt} = Q_{3,x} - b\sigma_2, \quad M_{3,x} + b\tau_2 h_3/2 - Q_3 = 0,
\end{aligned} \tag{10}$$

where subscripts 1, 2 and 3 represent the upper actuator layer, the host beam and the lower actuator layer, respectively; u and w are the longitudinal and the transverse displacements, respectively; τ and σ are shear and peel stress of the adhesive layer; T, Q and M are the axial stress, shear stress and moment resultants, respectively; h denotes the thickness, b is the width of the composite beam, and ρ is the mass density.

Employing Eq. (9), the stress distribution of the ith layer can be expressed as

$$\sigma_i = Y_i(u_{i,x} - z_i w_{i,xx}) - p_{31i} I_i^{\beta}, \quad i = 1, 2, 3, \tag{11}$$

where z_i is the z-coordinate from the neutral plane of the actuator layer, Y_i is the Young's modulus of the ith layer, I_i is the light intensity. Note that for the host beam, $p_{312} = I_2 = 0$.

By integrating Eq. (11), the axial forces and bending moments for the three layers can be expressed by the generalized displacements, i.e.

$$T_i = A_i u_{i,x} - B_i w_{i,xx} - bp_{31i} h_i \tilde{I}_i, \quad M_i = B_i u_{i,x} - D_i w_{i,xx} - bp_{31i} r_i h_i \tilde{I}_i, \quad i = 1, 2, 3, \tag{12}$$

where r_i is the z-coordinate value of the mid-plane of the actuator layer from its own neutral plane of the composite beam, A_i and D_i the axial and bending stiffness, B_i the extension–bending coupling term, and $\tilde{I}_i = I_i^{\beta}$. It should be noted that the axial forces T_i and M_i include the contributions of the photostrictive actuators under light irradiation.

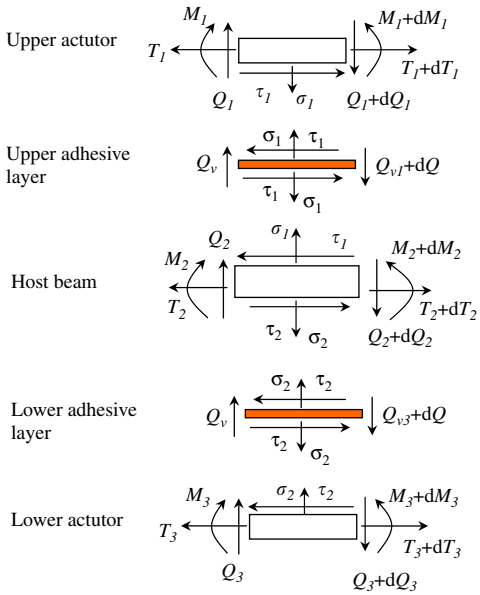

Fig. 4. Free body diagram of the infinitesimal element.

To transform Eq. (12) into homogeneous form, introducing

$$T_i^e = T_i + bp_{31i}h_i\tilde{I}_i, \quad M_i^e = M_i + bp_{31i}r_ih_i\tilde{I}_i \tag{13}$$

which represent the axial force and bending moment without the contribution of photostriction of the actuator. Substituting Eq. (13) into Eq. (12), we have

$$T_i^e = A_iu_{i,x} - B_iw_{i,xx}, \quad M_i^e = B_iu_{i,x} - D_iw_{i,xx}, \quad i = 1,2,3. \tag{14}$$

Since the light intensity is independent of x, we have replaced T_i and M_i in Eq. (14) with T_i^e and M_i^e without changing these equations.

Using the constant shear and peel strain assumption, the shear and peel stress in the adhesive layer are given by

$$\begin{aligned} \tau_i &= \frac{Y_{vi}}{2(1+v_{vi})h_{vi}}[(h_iw_{i,x} + h_{i+1}w_{i+1,x})/2 + (u_{i+1} - u_i)], \\ \sigma_i &= \frac{Y_{vi}(1-v_{vi})}{(1-2v_{vi})(1+v_{vi})h_{vi}}(w_{i+1} - w_i), \end{aligned} \qquad i = 1,2, \tag{15}$$

where h_v is the thickness of the adhesive layers, Y_v and v_v are the Young's modulus and Poisson's ratio of the adhesive layer, respectively.

Substituting the peel and shear stresses in Eq. (15) into Eqs. (10) and (14), we can obtain 15 equations of the composite segment in terms of the displacements and general forces. Introducing state vectors that consist of these displacements and general forces

$$\mathbf{y}_i = (u_i, T_i^e, w_i, \psi_i, Q_i, M_i)^{\mathrm{T}}, \quad i = 1,2,3, \quad \mathbf{y} = (\mathbf{y}_1^{\mathrm{T}}, \mathbf{y}_2^{\mathrm{T}}, \mathbf{y}_3^{\mathrm{T}})^{\mathrm{T}}, \tag{16}$$

where $\psi_i = w_{i,x}$ is the rotational angle and supplementing equations $w_{i,x} = \psi_i$ $(i = 1,2,3)$, these equations in Eqs. (10) and (14) can be rewritten in the following matrix form:

$$\mathbf{M}\mathbf{y}_{,tt} - \mathbf{y}_{,x} + \mathbf{K}\mathbf{y} = \mathbf{0}, \quad x_A \leqslant x \leqslant x_B, \tag{17}$$

where $\mathbf{M} \in R^{18\times18}$ and $\mathbf{K} \in R^{18\times18}$ are coefficient matrices.

For the segment without photostrictive actuators, its equations of motion can be obtained by simply dropping out the terms related to actuators. These six equations can be expressed as

$$\mathbf{M}_2\mathbf{y}_{2,x} - \mathbf{y}_{2,x} + \mathbf{K}_2\mathbf{y}_2 = \mathbf{0}, \quad 0 \leqslant x \leqslant x_A, \quad x_B \leqslant x \leqslant l, \tag{18}$$

where $\mathbf{M}_2 \in R^{6\times6}$ and $\mathbf{K}_2 \in R^{6\times6}$ are coefficient matrices of the host beam.

3.2. Boundary and continuity conditions

The boundary conditions for the host beam can be written in the following general form:

$$\mathbf{D}_{l2}\mathbf{y}_2(0) + \mathbf{D}_{r2}\mathbf{y}_2(l) = \mathbf{d}_2, \tag{19}$$

where $\mathbf{D}_{l2} \in R^{6\times6}$, $\mathbf{D}_{r2} \in R^{6\times6}$ are constant matrices, and $\mathbf{d}_2 \in R^6$ is a known vector. Similarly, the boundary conditions for the photostrictive actuators can be expressed by

$$\mathbf{D}_{li}\mathbf{y}_i(x_A) + \mathbf{D}_{ri}\mathbf{y}_i(x_B) = \tilde{I}_i\mathbf{d}_i, \quad i = 1,3, \tag{20}$$

where $\mathbf{D}_{li} \in R^{6\times6}$, $\mathbf{D}_{ri} \in R^{6\times6}$ are constant matrices, and $\mathbf{d}_2 \in R^6$ is a known vector for the actuator patches, $\mathbf{d}_1 \in R^6$ and $\mathbf{d}_3 \in R^6$ are constant vectors. For a free–free photostrictive film actuator, $T_i = Q_i = M_i = 0$, i.e. $Q_i = 0$, $T_i^e = bp_{31i}h_i\tilde{I}_i$ and $M_i^e = bp_{331}r_ih_i\tilde{I}_i$. These boundary conditions can be expressed using Eq. (20) with

the following coefficient matrices and vector:

$$\mathbf{D}_{li}=\begin{bmatrix}0&1&0&0&0&0\\0&0&0&0&1&0\\0&0&0&0&0&1\\0&0&0&0&0&0\\0&0&0&0&0&0\\0&0&0&0&0&0\end{bmatrix},\quad \mathbf{D}_{ri}=\begin{bmatrix}0&0&0&0&0&0\\0&0&0&0&0&0\\0&0&0&0&0&0\\0&1&0&0&0&0\\0&0&0&0&1&0\\0&0&0&0&0&1\end{bmatrix},\quad \mathbf{d}_i=bp_{31i}h_i\begin{bmatrix}1\\0\\r_i\\1\\0\\r_i\end{bmatrix}. \tag{21}$$

The continuity conditions of the host beam at the interfaces x_A and x_B should be imposed to maintain the continuity of displacements and the equilibrium of forces.

3.3. Sensor equation of laser Doppler vibrometer

To perform wireless remote vibration control of flexible structures, remote sensors are needed. Laser Doppler vibrometers remotely measure velocities and displacements of a vibrating object by sending monochromatic laser beam toward the target object and collecting the reflected radiation. According to the Doppler effect, the change in frequency (or wavelength) of the reflected radiation is a function of the relative velocity of the target object. Thus, the velocity of the object can be obtained by measuring the change in frequency of the reflected laser light. Laser vibrometers are light-based sensors, and they are ideal to be used as remote sensors in wireless vibration control of structures incorporating with the photostrictive actuators.

When a laser beam is perpendicular to the beam at its rest position, the output voltage of the laser vibrometer is given by

$$U(t)=k[w_{,t}(x_C,t)\cos\psi+u_{,t}(x_C,t)\sin\psi], \tag{22}$$

where $\psi(x_C,t)$ is the rotational angle at the measuring point C.

For a vibration with small amplitude, Eq. (22) can be simplified as

$$U(t)=kw_{,t}(x_C,t). \tag{23}$$

Eq. (23) shows that the laser Doppler vibrometer senses the transverse velocity of host beam when the laser beam is perpendicular to the host beam. This sensing equation will be used to perform wireless remote vibration control of beams incorporating with photostrictive actuators.

4. Wireless remote control scheme

Due to the limitation of response speed of photostrictive actuators, active vibration control will focus on the control of the first several dominant modes with lower modal frequencies. To do so, the desired modal velocity for a given mode need to be observed from the sensed signal that is a superposition of all modal velocities. A modal velocity filter (MVF) is designed to obtain the designated modal velocity for the vibration velocity sensed by the laser vibrometer. The MVF is developed based on two second-order systems and has the following form:

$$\begin{aligned}&y_{1,tt}(t)+2\omega_c\zeta_{c1}y_{1,t}(t)+\omega_c^2y_1(t)=\omega_c^2U(t),\\&y_{2,tt}(t)+2\omega_c\zeta_{c2}y_{2,t}(t)+\omega_c^2y_2(t)=y_{1,tt}(t),\end{aligned} \tag{24}$$

where ω_c is the frequency of the second-order systems, and ζ_{c1} and ζ_{c2} are the damping ratios of the two second-order systems, respectively. The input of the second system is the acceleration output of the first system. The complex frequency response function of Eq. (24) is

$$H(\lambda)=\frac{\lambda^2}{[1-\lambda^2+2\mathrm{j}\zeta_{c1}\lambda][1-\lambda^2+2\mathrm{j}\zeta_{c2}\lambda]}, \tag{25}$$

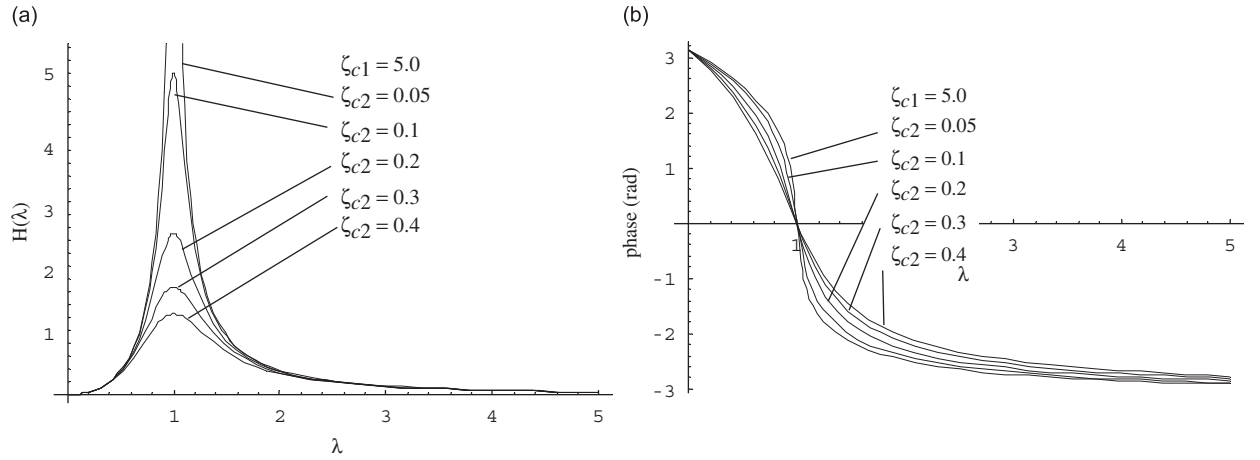

Fig. 5. Amplitude and phase of response of MVF versus frequency. (a) Amplitude-frequency curve, (b) phase–frequency curve.

where $\lambda = \omega/\omega_c$ is the frequency ratio, and $j = \sqrt{-1}$. The amplitude–frequency and phase–frequency curves are depicted in Fig. 5. As shown in Fig. 5a, the component in the input $U(t)$ whose frequency is very close to that of the second-order systems is amplified, whereas those whose frequencies are much lower or higher than the frequency of the MVF are depressed. Therefore, Eq. (24) functions as a special bandpass filter. Fig. 5b shows that the phase difference between the output of MVF and the input at $\lambda = 1$ is zero. This indicates that the response of the MVF to the input $U(t)$ is proportional to the desired velocity component by making its natural frequency ω_c equal to the designated modal frequency of the structures to be controlled.

To actively control vibration of the beam using photostrictive actuators, the control light intensity should be designed according to some control laws. To control the ith mode of the composite beam, the ith modal velocity, which is proportional to the output $y_2(\omega_i, t)$of the MVF, can be used to form the control light intensity on the upper actuator as

$$\tilde{I}_1(t) = -g y_2(\omega_i, t), \tag{26}$$

where g is the control gain, ω_i is the ith modal frequency of the beam, and $y_2(\omega_i,t)$ is the response of the MVF with a natural frequency ω_i to the sensed signal of the laser vibrometer $U(t)$.

To control the lowest N modes simultaneously, the feedback control light intensity is designed by

$$\tilde{I}_1(t) = -\sum_{i}^{N} g_i y_2(\omega_i, t), \tag{27}$$

where g_i is the control gain for the ith mode.

However, the light intensity is non-negative, Eq. (27) in practise is modified as

$$\tilde{I}_1(t) = \tilde{I}_0 - \sum_{i}^{N} g_i y_2(\omega_i, t), \tag{28}$$

where $I_0 > |g y_2(\omega_i, t)|$ for $\forall t$. To balance the static deflection caused by the constant light intensity $\tilde{I}_0$ applied on the upper actuator, the same constant light intensity should be also applied onto the lower actuator, i.e.

$$\tilde{I}_2(t) = \tilde{I}_0. \tag{29}$$

The block diagram of the independent modal control using wireless remote sensors and actuators is shown in Fig. 6.

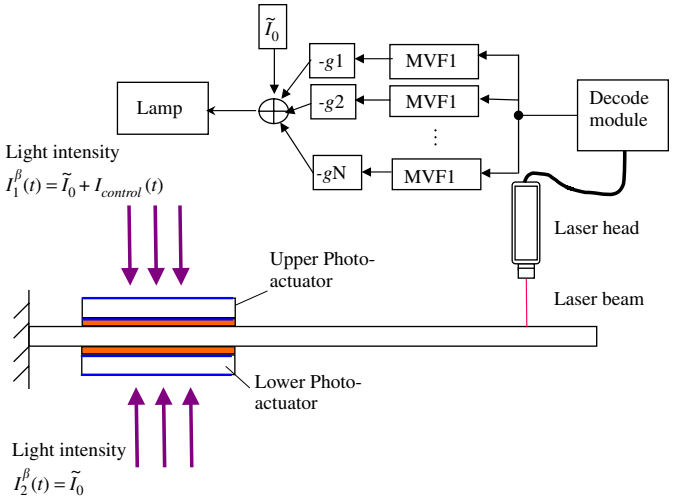

Fig. 6. Block diagram of wireless remote control using light-based sensors and actuators.

5. Generalized modal analysis

To examine the control effect of the wireless remote control system, the eigenvalues of the closed-loop controlled system should be determined. In doing so, performing Laplace transformation with respect to time t of Eq. (17) gives

$$\bar{\mathbf{y}}_{,x} = \bar{\mathbf{K}}(s)\bar{\mathbf{y}}, \quad x_A \leqslant x \leqslant x_B, \tag{30}$$

where $\bar{\mathbf{K}}(s) = \mathbf{K} - s^2\mathbf{M}$, s is the transformation coefficient, and $\bar{\mathbf{y}}(x,s)$ represents the transformation of $\mathbf{y}(x,t)$. The solution of Eq. (30) is

$$\bar{\mathbf{y}}(x,s) = \bar{\mathbf{y}}(x_A,s)\exp[\bar{\mathbf{K}}(x - x_A)], \quad x_A \leqslant x \leqslant x_B. \tag{31}$$

Similarly, for the host beam, we have

$$\begin{aligned} \bar{\mathbf{y}}_2(x,s) &= \bar{\mathbf{y}}_2(0,s)\exp(\bar{\mathbf{K}}_2 x), \quad 0 \leqslant x \leqslant x_A, \\ \bar{\mathbf{y}}_2(x,s) &= \bar{\mathbf{y}}_2(x_B,s)\exp[\bar{\mathbf{K}}_2(x - x_B)], \quad x_B \leqslant x \leqslant l. \end{aligned} \tag{32}$$

If $\bar{\mathbf{y}}(x_A,s)$, $\bar{\mathbf{y}}_2(0,s)$ and $\bar{\mathbf{y}}_2(x_B,s)$ are determined, the responses of the beam in s-plane to the light irradiation at all segments can be obtained from Eqs. (31) and (32). These state vectors at interfaces and boundaries can be obtained by solving the following algebraic equations, in which the Laplace transformation of the response at the sensing point x_C, boundary and continuity conditions are included

$$\begin{aligned} &\bar{\mathbf{y}}_2(x_A,s) = \bar{\mathbf{y}}_2(0,s)\ \exp(\bar{\mathbf{K}}_2 x_A), \\ &\bar{\mathbf{y}}(x_B,s) = \bar{\mathbf{y}}(x_A,s)\ \exp[\bar{\mathbf{K}}(x_B - x_A)], \\ &\bar{\mathbf{y}}_2(x_C,s) = \bar{\mathbf{y}}_2(x_B,s)\ \exp[\bar{\mathbf{K}}_2(x_C - x_B)], \\ &\bar{\mathbf{y}}_2(l,s) = \bar{\mathbf{y}}_2(x_C,s)\ \exp[\bar{\mathbf{K}}_2(l - x_C)], \\ &\mathbf{G}\mathbf{y}(x_A,s) = \mathbf{y}_2(x_A,s), \\ &\mathbf{G}\mathbf{y}(x_B,s) = \mathbf{y}_2(x_B,s), \\ &\mathbf{D}_{l2}\bar{\mathbf{y}}_2(0) + \mathbf{D}_{r2}\bar{\mathbf{y}}_2(l) = \mathbf{0}, \\ &\mathbf{D}_{l1}\bar{\mathbf{y}}_1(x_A) + \mathbf{D}_{r1}\bar{\mathbf{y}}_1(x_B) = \bar{I}_1\mathbf{d}_1, \\ &\mathbf{D}_{l3}\mathbf{y}_3(x_A) + \mathbf{D}_{r3}\mathbf{y}_3(x_B) = \bar{I}_3\mathbf{d}_3, \end{aligned} \tag{33}$$

where $\bar{I}_1(s)$ is the Laplace transformation of $\tilde{I}_1(t)$, $\mathbf{G}$ is a transformation matrix given by

$$\mathbf{G} = \begin{bmatrix} \mathbf{0}_6 & \mathbf{0}_6 & \mathbf{0}_6 \\ \mathbf{0}_6 & \mathbf{n}_6 & \mathbf{0}_6 \\ \mathbf{0}_6 & \mathbf{0}_6 & \mathbf{0}_6 \end{bmatrix} \tag{34}$$

in which $\mathbf{0}_6$ is a 6×6 zero matrix, and $\mathbf{n}_6$ is 6×6 identity matrix.

The Laplace transformation of the light intensity can be obtained from Eqs. (24) and (27)

$$\bar{I}_1(s) = -\bar{U}(s)\sum_{i}^{N} g_i H_i(s), \quad \bar{I}_3 = 0, \tag{35}$$

where

$$H_i(s) = \frac{\omega_c^2 s^2}{[\omega_i^2 + s^2 + 2\zeta_{c1}\omega_i s][\omega_i^2 + s^2 + 2\zeta_{c2}\omega_i s]}. \tag{36}$$

From Eq. (23), $\bar{U}(s)$ can be expressed as

$$\bar{U}(s) = ks\bar{w}_2(x_C, s) = ks\mathbf{R}\,\bar{\mathbf{y}}_2(x_C, s), \tag{37}$$

where $\mathbf{R} = \begin{bmatrix} 0 & 0 & 1 & 0 & 0 & 0 \end{bmatrix}$ is a 1×6 transformation matrix. Substituting Eqs. (35) and (37) into the boundary conditions of the upper and lower actuators gives

$$\begin{aligned} &\mathbf{D}_{l1}\bar{\mathbf{y}}_1(x_A) + \mathbf{D}_{r1}\bar{\mathbf{y}}_1(x_B) + \mathbf{Z}(s)\bar{\mathbf{y}}_2(s) = 0, \\ &\mathbf{D}_{l3}\mathbf{y}_3(x_A) + \mathbf{D}_{r3}\mathbf{y}_3(x_B) = 0, \end{aligned} \tag{38}$$

where $\mathbf{Z}(s) = [ks\sum_{i=1}^{N} g_i H_i(s)]\mathbf{d}_1\,\mathbf{R}$ is a 6×6 matrix related to the feedback control. Replacing boundary conditions of the actuators in Eq. (33) with Eq. (38), and rewriting the equations in matrix form, we have

$$\mathbf{\Phi}(s)\bar{\mathbf{y}}_{\text{int}}(s) = 0, \tag{39}$$

where

$$\mathbf{\Phi}(s) = \begin{bmatrix} \exp(\bar{\mathbf{K}}_2 x_A) & \mathbf{0} & -\mathbf{n} & \mathbf{0} & \mathbf{0} & \mathbf{0} & \mathbf{0} & \mathbf{0} & \mathbf{0} \\ \mathbf{0} & \mathbf{L}_{11} & \mathbf{L}_{12} & \mathbf{L}_{13} & -\mathbf{n} & \mathbf{0} & \mathbf{0} & \mathbf{0} & \mathbf{0} \\ \mathbf{0} & \mathbf{L}_{21} & \mathbf{L}_{22} & \mathbf{L}_{23} & \mathbf{0} & -\mathbf{n} & \mathbf{0} & \mathbf{0} & \mathbf{0} \\ \mathbf{0} & \mathbf{L}_{31} & \mathbf{L}_{32} & \mathbf{L}_{33} & \mathbf{0} & \mathbf{0} & -\mathbf{n} & \mathbf{0} & \mathbf{0} \\ \mathbf{0} & \mathbf{0} & \mathbf{0} & \mathbf{0} & \mathbf{0} & \exp[\bar{\mathbf{K}}_2(x_C - x_B)] & \mathbf{0} & -\mathbf{n} & \mathbf{0} \\ \mathbf{0} & \mathbf{0} & \mathbf{0} & \mathbf{0} & \mathbf{0} & \mathbf{0} & \mathbf{0} & \exp[\bar{\mathbf{K}}_2(x_C - x_B)] & -\mathbf{n} \\ \mathbf{0} & \mathbf{D}_{l1} & \mathbf{0} & \mathbf{0} & \mathbf{D}_{r1} & \mathbf{0} & \mathbf{0} & \mathbf{Z} & \mathbf{0} \\ \mathbf{0} & \mathbf{0} & \mathbf{0} & \mathbf{D}_{l3} & \mathbf{0} & \mathbf{0} & \mathbf{D}_{r3} & \mathbf{0} & \mathbf{0} \\ \mathbf{D}_{l2} & \mathbf{0} & \mathbf{0} & \mathbf{0} & \mathbf{0} & \mathbf{0} & \mathbf{0} & \mathbf{0} & \mathbf{D}_{r2} \end{bmatrix},$$

$$\bar{\mathbf{y}}_{\text{int}} = [\mathbf{y}_2(0), \mathbf{y}_1(x_A), \mathbf{y}_2(x_A), \mathbf{y}_3(x_A), \mathbf{y}_1(x_B), \mathbf{y}_2(x_B), \mathbf{y}_3(x_B), \mathbf{y}_2(x_C), \mathbf{y}_2(l)]^{\mathrm{T}}, \tag{40}$$

where $\mathbf{L}_{ij}$ is the sub-matrix of $\exp[\bar{\mathbf{K}}(x_B - x_A)]$, $\mathbf{0}$ is a 6×6 zero matrix, and $\mathbf{n}$ is a 6×6 identity matrix.

To obtain a non-trivial solution of $\bar{\mathbf{y}}_{\text{int}}$, the following condition must hold:

$$\det[\mathbf{\Phi}(s)] = 0. \tag{41}$$

Eq. (41) is a transcendental equation known as characteristic equation for the closed-loop control system, which can give complex eigenvalues of the controlled beam. If all the eigenvalues have non-positive real parts, the control of the beam is stable.

6. An illustrative example

As an illustrative example, we consider a cantilever beam bonded with two identical photostrictive actuator films on its upper and lower surfaces. The host beam is a thin aluminum beam with dimensions of $300\,\text{m} \times 5\,\text{mm} \times 0.8\,\text{mm}$. The Young's modulus of the host beam is 70 GPa, and its mass density is $2700\,\text{kg/m}^3$. The thickness of the thin adhesive layer is 0.1 mm, and its Young's modulus and mass density are 2 GPa and $1250\,\text{kg/m}^3$, respectively. The photostrictive actuator films are made of PLZT (3/52/48) ceramics with dimensions of $30\,\text{mm} \times 5\,\text{mm} \times 0.3\,\text{mm}$. The upper and lower surfaces of the actuator film are coated by indium tin oxide as transparent electrodes, and it is polarized in the thickness direction. Since the electrodes are transparent, they are able to receive light illumination. The Young's modulus of the PLZT is 68 GPa, and its mass density is $7600\,\text{kg/m}^3$. The piezoelectric strain constant of the PLZT is $175 \times 10^{-12}\,\text{m/V}$. The photovoltage of this material is proportional to the square root of light intensity [4], i.e.,

$$\bar{E} = p_{33} I_{\text{op}}^{0.5}, \tag{42}$$

where $p_{33} = 20.87\,\text{V/W}^{0.5}$.

The laser Doppler vibrometer (Polytec CLV 1222) has a sensitivity of 5 mm/s/V, from which the amplifying factor can be calculated as $k = 200\,\text{V/m/s}$. The laser head of the Doppler vibrometer is fixed in such a location that it can sense the velocity at the point 5 cm from the free end of the host beam.

For the uncontrolled beam, the first four eigenvalues obtained from Eq. (41) are 53.5j, 294.2j, 704.4j and 1354.3j, respectively, which indicates that the first five modal frequencies of the beam is 8.5, 46.8, 112.1 and 215.6 Hz, respectively. Since the natural damping is not considered in this example, the damping ratios for any control mode of the uncontrolled beam is zero.

In the close-loop control, we will control the first two modes using the photostrictive actuators due to its limitation of response speed. To control the first mode using the control law given in Eq. (26), the coefficients in the MVF are chosen as $\omega_c = 53.5\,\text{rad/s}$, $\zeta_{c1} = 0.5$, $\zeta_{c2} = 0.7$. When the control gain g_1 is selected as 500, the obtained eigenvalues for the controlled beam are listed in Table 1. The first mode is controlled effectively since its damping ratio has been changed from zero in the uncontrolled case to 0.018 in the controlled case. Due to increase in the active damping ratio, the imaginary part of the first eigenvalue is slightly reduced, which indicates the first damped frequency is smaller than the first natural frequency. It should be noted that the closed-loop control designed for controlled the first mode also slightly affects the residual modes. For example, it increases the damping ratios of the second modes, but decreases the third and fourth modes. Since these changes of damping ratio caused by the first mode controller are very small compared to their natural damping ratios, the residual mode will still remain stable.

To control the second mode, we use the same damping ratios for the MVF used for controlling the first mode and $\omega_c = 299.5\,\text{rad/s}$. When the control gain g_2 is chosen as 400, the obtained eigenvalues of the controlled beam is presented in Table 2. Since the MVF is designed to observe the second modal velocity, the second mode is effectively controlled by the closed-loop control system. The second modal damping ratio for the controlled beam is increased to 0.005. Although the residual modes are also slightly affected, but the changes of their damping ratios are very small.

The active damping ratio of each controlled mode is dependent on the control gain. Fig. 7 depicts the relationship between the active damping ratios of the first two controlled modes and the control gains. It shows that the active damping ratios become larger as the control gains increase. However, the relationship between the damping ratio and the control gain exhibits slightly hardening nonlinear behavior.

When the control gains in Eq. (27) are chosen as $g_1 = 500$ and $g_2 = 400$, the first two dominant modes will be controlled simultaneously and the obtained eigenvalues as well as their corresponding damping ratios are given in Table 3. As shown in Table 3, the damping ratios for mode l and mode 2 have been significantly increased, which indicates that these two modes are effectively controlled by the wireless modal control system. The damping ratios of the residual modes are hardly affected by the closed-loop control. For example, the damping ratios for the third and fourth modes are -0.00004 and 0.00003, respectively. This means that the control energy has been used to control the target modes. The slight changes of the damping ratios of the residual modes result from the observation spillover of the MVF. Although the observation spillover may

Table 1
The eigenvalues for the beam with the first mode controlled

Mode no.	Eigenvalue	Damped frequency (Hz)	Damping ratio
1	−0.95 + 53.4j	8.50	0.018
2	−0.01 + 294.2j	46.82	0.00004
3	−0.001 + 704.4j	112.11	0
4	0.0017 + 1354.3j	215.55	0

Table 2
The eigenvalues for the beam with the second mode controlled

Mode no.	Eigenvalue	Damped frequency (Hz)	Damping ratio
1	−0.004 + 53.4j	8.50	0.000076
2	−1.5 + 294.2j	46.82	0.005
3	0.03 + 704.4j	112.11	−0.00004
4	−0.04 + 1354.3j	215.55	0.00003

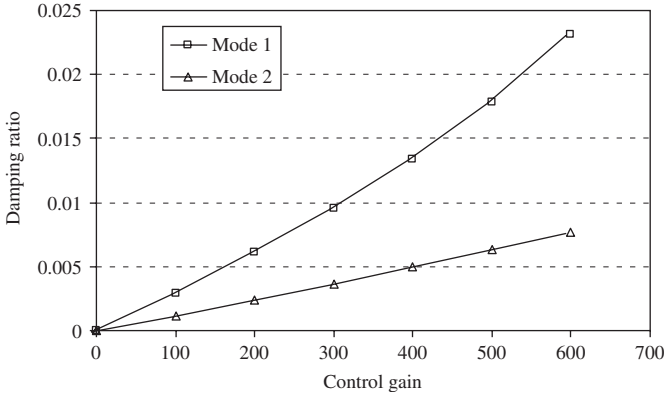

Fig. 7. Modal damping ratio via control gains.

result in small negative damping ratios for some of the residual modes, which theoretically indicates these modes are not stable, these modes will remain stable in engineering practice because their natural damping ratios will be much larger than these negative damping ratios caused by the controller.

7. Conclusion

This paper investigates wireless remote vibration control of flexible beams using light-driven photostrictive actuators incorporating with a laser Doppler vibrometer. The actuating equation of the photostrictive actuators is derived to establish the relationship between the motion of the host beam and the input light intensity exerted on the actuator patch. A sensing equation of the laser Doppler vibrometer is also given to describe the relationship between the output of the vibrometer and velocity of the vibrating beam. A modal velocity filter (MVF) is employed to perform independent modal control of the beam using the light-based actuator and sensor. To examine the control effect, a characteristic equation is presented from which the frequencies and active damping ratios for all modes can be evaluated. Finally, a simulation example is presented to show the effectiveness of the present model and control scheme. Simulation results show that the control photostrictive actuators are suitable for controlling lower modes of flexible beams.

Table 3
The eigenvalues for the beam with the first two modes controlled

Mode no.	Eigenvalue	Damped frequency (Hz)	Damping ratio
1	−0.96 + 53.4j	8.50	0.018
2	−1.47 + 294.2j	46.82	0.005
3	0.03 + 704.4j	112.11	−0.00004
4	−0.04 + 1354.3j	215.55	0.00003

Acknowledgement

This research was supported by the Australian Research Council through Discovery-Projects grants (DP0346419, DP0774596).

References

[1] E.F. Crawley, Intelligent structures for aerospace: a technology overview and assessment, *AIAA Journal* 32 (8) (1994) 1689–1699.
[2] C. Chee, L. Tong, G.P. Steven, A review on the modeling of piezoelectric sensors and actuators incorporated in intelligent structures, *Journal of Intelligent Material Systems and Structures* 9 (1) (1998) 3–19.
[3] K. Nonaka, M. Akiyama, T. Hagio, A. Takase, Effect of multiple impurity doping on the photovoltaic properties of lead zirconate–titanate ceramics, *Ferroelectrics* 223 (1–4) (1999) 357–364.
[4] L.J. Zhou, A. Zimmermann, Y.P. Zeng, F. Aldinger, Effects of PbO content on the sintering behavior, microstructure, and properties of La-doped PZST antiferroelectric ceramics, *Journal of Materials Science-Materials in Electronics* 15 (3) (2004) 145–151.
[5] T. Fukuda, S. Hattori, F. Arai, H. Nakamura, Performance improvement of optical actuator by double side irradiation, *IEEE Transactions on Industrial Electronics* 42 (5) (1995) 455–461.
[6] K. Uchino, New applications of photostrictive ferroics, *Materials Research Innovations* 1 (3) (1997) 163–168.
[7] Y. Morikawa, T. Nakada, Bimorph-type optical actuator using PLZT elements—(position control of optical actuator by on-off control), *JSME International Journal Series C—Mechanical Systems* 41 (4) (1998) 860–866.
[8] G. Belforte, G. Eula, C. Ferraresi, et al., Mechanical microactuators with photostrictive control, *JSME International Journal Series C—Mechanical Systems* 41 (4) (1998) 886–892.
[9] S. Baglio, S. Castorina, L. Fortuna, N. Savalli, Modeling and design of novel photo-thermo-mechanical microactuators, *Sensors and Actuators A—Physical* 101 (1–2) (2002) 185–193.
[10] K. Kawaguchi, M. Ichiki, Y. Morikawa, T. Nakada, Electrical properties of photovoltaic PLZT and its application to optical motors, *Ferroelectrics* 273 (2002) 41–46.
[11] H.S. Tzou, C.S. Chou, Nonlinear opto-electromechanics and photodeformation of optical actuators, *Smart Materials and Structures* 5 (1996) 230–235.
[12] M. Ichiki, Y. Morikawa, Y. Mabune, T. Nakada, K. Nonaka, R. Maeda, Preparation and photo-induced properties of lead lanthanum zirconate titanate multilayers, *Journal of Physics, D: Applied Physics* 37 (2004) 3017–3024.
[13] P. Poosanaas, K. Tonooka, K. Uchino, Photostrictive actuators, *Mechatronics* 10 (2000) 467–487.
[14] C. Kittel, *Introduction to Solid States Physics*, seventh ed., Wiley, New York, 1996.